



**HAL**  
open science

## Elevation-induced climate change as a dominant factor causing the late Miocene C 4 plant expansion in the Himalayan foreland

Haibin Wu, Zhengtang Guo, Joel Guiot, Christine Hatté, Changhui Peng, Yanyan Yu, Juyi Ge, Qin Li, Aizhi Sun, Deai Zhao

### ► To cite this version:

Haibin Wu, Zhengtang Guo, Joel Guiot, Christine Hatté, Changhui Peng, et al.. Elevation-induced climate change as a dominant factor causing the late Miocene C 4 plant expansion in the Himalayan foreland. *Global Change Biology*, 2014, 20 (5), pp.1461-1472. 10.1111/gcb.12426 . insu-02269748

**HAL Id: insu-02269748**

**<https://insu.hal.science/insu-02269748>**

Submitted on 23 Aug 2019

**HAL** is a multi-disciplinary open access archive for the deposit and dissemination of scientific research documents, whether they are published or not. The documents may come from teaching and research institutions in France or abroad, or from public or private research centers.

L'archive ouverte pluridisciplinaire **HAL**, est destinée au dépôt et à la diffusion de documents scientifiques de niveau recherche, publiés ou non, émanant des établissements d'enseignement et de recherche français ou étrangers, des laboratoires publics ou privés.

Received Date : 04-Jan-2013  
Accepted Date : 14-Aug-2013  
Article type : Primary Research Articles

## **Elevation-induced climate change as a dominant factor causing the late Miocene C<sub>4</sub> plant expansion in the Himalayan foreland**

Haibin Wu<sup>1#</sup>, Zhengtang Guo<sup>1</sup>, Joël Guiot<sup>2</sup>, Christine Hatté<sup>3</sup>, Changhui Peng<sup>4,5</sup>, Yanyan Yu<sup>1</sup>, Juyi Ge<sup>1</sup>, Qin Li<sup>1</sup>, Aizhi Sun<sup>1</sup>, Deai Zhao<sup>1</sup>

<sup>1</sup>*Key Laboratory of Cenozoic Geology and Environment, Institute of Geology and Geophysics, Chinese Academy of Sciences, P.O. Box 9825, Beijing 100029, China*

<sup>2</sup>*Aix-Marseille Université, CNRS, IRD, CEREGE UM34, Europôle de l'Arbois BP 80, F-13545, Aix-en-Provence cedex 4, France*

<sup>3</sup>*Laboratoire des Sciences du Climat et de l'Environnement, UMR CEA-CNRS-UVSQ 8212, Domaine du CNRS, 91198 Gif-sur-Yvette, France*

<sup>4</sup>*Institute of Environment Sciences, Department of Biology Sciences, University of Quebec at Montreal (UQAM), Montreal, Canada*

<sup>5</sup>*Laboratory for Ecological Forecasting and Global Change, College of Forestry, Northwest A & F University, Yangling, Shaanxi 712100, China*

Resubmitted to “*Global Change Biology*”

# Correspondence should be addressed to:

Dr. Haibin Wu, Institute of Geology and Geophysics, Chinese Academy of Sciences, P.O. Box 9825, Beijing 100029, China

E-mail: Haibin-wu@mail.iggcas.ac.cn

Tel: +86 10 82998372; Fax: +86 10 88871410

This article has been accepted for publication and undergone full peer review but has not been through the copyediting, typesetting, pagination and proofreading process, which may lead to differences between this version and the Version of Record. Please cite this article as doi:

10.1111/gcb.12426

This article is protected by copyright. All rights reserved.

## Abstract

During the late Miocene, a dramatic global expansion of C<sub>4</sub> plant distribution occurred with broad spatial and temporal variations. Although the event is well documented, whether subsequent expansions were caused by a decreased atmospheric CO<sub>2</sub> concentration or climate change is a contentious issue. In the present study, we used an improved inverse vegetation modeling approach that accounts for the physiological responses of C<sub>3</sub> and C<sub>4</sub> plants to quantitatively reconstruct the paleoclimate in the Siwalik of Nepal based on pollen and carbon isotope data. We also studied the sensitivity of the C<sub>3</sub> and C<sub>4</sub> plants to changes in the climate and the atmospheric CO<sub>2</sub> concentration. We suggest that the expansion of the C<sub>4</sub> plant distribution during the late Miocene may have been primarily triggered by regional aridification and temperature increases. The expansion was unlikely caused by reduced CO<sub>2</sub> levels alone. Our findings suggest that this abrupt ecological shift mainly resulted from climate changes related to the decreased elevation of the Himalayan foreland.

**Keywords:** C<sub>4</sub> plant expansion, inverse vegetation model, paleoclimate reconstruction, pollen biome, late Miocene

## 1. Introduction

The expansion of plants characterized by the C<sub>4</sub> photosynthetic pathway during the late Tertiary was a major paleoecological event in Earth's terrestrial history (Cerling *et al.*, 1997; Sage, 2004; Tipple & Pagani, 2007). The C<sub>3</sub> and C<sub>4</sub> photosynthetic pathways fractionate carbon isotopes to different degrees: C<sub>3</sub> plants have  $\delta^{13}\text{C}$  values from -22‰ to -30‰, whereas C<sub>4</sub> plants have values from -10‰ to -14‰ (Bender, 1971; Farquhar *et al.*, 1983). Based on the analyses of carbon

This article is protected by copyright. All rights reserved.

isotopes in pedogenic carbonates, tooth enamel, and specific organic compounds, researchers have documented a significant expansion of the distribution of C<sub>4</sub> plants during the late Miocene in southern Asia, Africa, North America, and South America. The expansion first occurred at low latitudes and then later at higher latitudes (i.e., Quade *et al.*, 1989; Cerling *et al.*, 1997; Huang *et al.*, 2007; Zhang *et al.*, 2009).

This expansion has been explained by a large reduction in the atmospheric CO<sub>2</sub> concentration during the late Miocene (Cerling *et al.*, 1997); C<sub>4</sub> plants possess a CO<sub>2</sub>-concentrating mechanism and are favored relative to C<sub>3</sub> plants under low levels of atmospheric CO<sub>2</sub>. However, recent reconstructions of paleo-atmospheric CO<sub>2</sub> concentrations indicate that a precipitous drop in CO<sub>2</sub> levels had already occurred during the Oligocene; the levels approached modern levels by the earliest Miocene period (Pearson & Palmer, 2000; Pagani *et al.*, 2005), which is earlier than the global expansion of C<sub>4</sub> plants. In addition, detailed studies suggest that the late Miocene expansion of C<sub>4</sub> plants was regionally heterogeneous rather than globally synchronous (Fox & Koch, 2003, 2004; Huang *et al.*, 2007; Edwards & Still, 2008; Sanyal *et al.*, 2010). Regional climatic factors may have superimposed to global CO<sub>2</sub> levels to control the expansion. The relative importance of these factors needs to be investigated in more detail to better identify the causes of the C<sub>4</sub> expansion in various regions.

Physiological data and models have demonstrated that the processes that modify the distributions of C<sub>3</sub> and C<sub>4</sub> plants strongly depend on both the atmospheric CO<sub>2</sub> concentration and seasonal climate changes (Collatz *et al.*, 1998; Edwards & Still, 2008; Higgins & Simon, 2012). Therefore, to establish the primary cause of the late Miocene expansion of the C<sub>4</sub> plant distribution, it is

important to identify the underlying causes based on the physiological responses of the C<sub>3</sub> and C<sub>4</sub> plants by accounting for atmospheric CO<sub>2</sub> levels and seasonal climate changes. The results will elucidate the relative influences of these various factors on the expansion.

In this study, we describe the use of an inverse vegetation model that is based on a physiological process-based vegetation model (BIOME4) (Kaplan *et al.*, 2003), pollen data (Hoorn *et al.*, 2000), and carbon isotope data (Quade *et al.*, 1995) from the Nepal Siwalik region in the Himalayan foreland. In this region, major C<sub>4</sub> plant distribution expansion has occurred since the late Miocene. We quantitatively reconstructed the paleoclimates during that period and investigated how changes in the atmospheric CO<sub>2</sub> concentration and seasonal climate changes account for the observed distribution of the C<sub>3</sub> and C<sub>4</sub> plants in this region.

## 2. Data

The Surai Khola section (27°45'27" N, 82°50' E) of the Siwalik, Central Nepal (Fig. 1), was studied to obtain detailed data on pollen (Hoorn *et al.*, 2000) and carbon isotopes (Quade *et al.*, 1995) in soil carbonates and soil organic matter. In the present study, all pollen and isotope data were obtained from published diagrams (Quade *et al.*, 1995; Hoorn *et al.*, 2000). Then, we precisely tied these data to the paleomagnetic age control data of Cande and Kent (1995). For the pollen sites, aquatic pollen or spores and fern spores were excluded, and the percentages were recalculated based on the arboreal and nonarboreal pollen types.

The biome reconstruction (Fig. 2a), which is based on the biomization method, was developed by MCQPD (2001). Because  $\delta^{13}\text{C}$  values of organic matter in Surai Khola (Fig. 2b) were scarce

(only two sites) prior to 6.5 Myr, the  $\delta^{13}\text{C}$  of soil pedogenic carbonates was used. We used a 15‰ enrichment of the  $\delta^{13}\text{C}$  in the soil carbonate compared to the source organic matter; this accounts for kinetic fractionation effects on  $\text{CO}_2$  as a result of diffusion and equilibrium fractionation during the  $\text{CO}_2$  to  $\text{CaCO}_3$  phase transformation (Quade *et al.*, 1995). Because the pollen and  $\delta^{13}\text{C}$  were not sampled together, the  $\delta^{13}\text{C}$  at pollen collection sites (Fig. 2) was interpolated using a five-point moving average from the  $\delta^{13}\text{C}$  of the soils to the age of the pollen sites. To evaluate the reliability of the inverse method for the climate reconstruction, modern pollen data were used from the available pollen spectra in China (MCQPD, 2001). The biome types include tropical rain forest, tropical seasonal forest, broadleaved evergreen/warm mixed forest, temperate deciduous forest, cool conifer forest, cold mixed forest, taiga, tundra, steppe, and desert, which cover all biome changes of the Surai Khola section. These biome and  $\delta^{13}\text{C}$  data are the output vectors from the inverse modeling simulations.

The model input vectors include parameters characterizing atmospheric  $\text{CO}_2$  concentration, atmospheric  $\delta^{13}\text{C}$ , soil texture, and monthly climate data for vegetation simulations. We used the reconstructed atmospheric  $\text{CO}_2$  concentration since the Miocene compiled by LaRiviere *et al.* (2012) and the atmospheric  $\delta^{13}\text{C}$  derived from Passey *et al.* (2002) (Fig. 3). Then, we interpolated the values to the pollen sites using a five-point moving average method. Due to the lack of paleosol data, the paleosol properties at the pollen collection sites were characterized by the nearest soil grid in the Surai Khola with the same biome at the present time. The soil properties were derived from the FAO digital soil map of the world (FAO, 1995). The modern monthly climate conditions (i.e., temperature, precipitation, sunshine) and absolute minimum temperatures were interpolated using a two-layer back-propagation artificial neural network

method (Guiot *et al.*, 1996), which is included in the 3Pbase software (Guiot & Goeury, 1996), based on the monthly climate dataset in the ten-minute grid space compiled by New *et al.* (2000) and the absolute minimum temperatures compiled by Spangler and Jenne (1988). The artificial neural network technique is able to simulate complex and non-linear relationships; therefore, it is able to represent (nevertheless as a black box) the spatial changes of climate (Guiot *et al.*, 1996). The inverse modeling process is performed using initial sampling increments from -20°C to +10°C of the modern temperatures and -90% to +100% of the modern precipitation values in January and July (Table 1).

### 3. Methods

A novel aspect of our approach (Fig. 4) was the use of a physiological process-based vegetation model, BIOME4 (Kaplan *et al.*, 2003), in an inverse mode to study the sensitivity of C<sub>3</sub> and C<sub>4</sub> plants to changes in climate and atmospheric CO<sub>2</sub> concentrations since the late Miocene. We assumed that the pollen biome and carbon isotope values, which reflect the composition and structure of the local C<sub>3</sub> and C<sub>4</sub> plants, are related to the simulated biome and carbon isotope results of BIOME4.

#### 3.1 BIOME4 vegetation model

BIOME4, modified from BIOME3 (Haxeltine & Prentice, 1996), is an equilibrium vegetation model that accounts for the effects of CO<sub>2</sub> on net assimilation, stomatal conductance, leaf area index (LAI), and ecosystem water balance. The model has been used to simulate the response of plants to changed atmospheric CO<sub>2</sub> in the past (Jolly & Haxeltine, 1997; Boom *et al.*, 2002; Harrison & Prentice, 2003; Wu *et al.*, 2007). The model includes 12 plant functional types (PFT)

This article is protected by copyright. All rights reserved.

defined by a set of bioclimatic limits and physiological parameters. These PFTs represent broad and physiologically distinct classes that range from cushion forbs to tropical rain forest trees. For a given site, the ecophysiological constraints determine the potential occurrence of specific PFTs. A coupled carbon and water flux scheme for each PFT is then used to calculate the seasonal maximum LAI that maximizes the net primary production (NPP). The scheme is based on a daily time-step simulation of the soil water balance and monthly process-based calculations of canopy conductance, photosynthesis, respiration, and phenological state. Competition between the PFTs is simulated by using the optimal NPP of each PFT as an index of competitiveness. To identify the biome of a given site, the model ranks the woody and grass PFTs that were calculated for the site. The ranking is based on a set of rules related to the biogeochemical variables (i.e., LAI, NPP, and annual mean soil moisture). The ranked combination of the PFTs is classified into one of 27 biome types.

BIOME4 also includes an isotopic fractionation routine that was improved by Hatté and Guiot (2005). The isotopic fractionation produced by  $C_3$  and  $C_4$  plants is simulated by using a model modified from Lloyd and Farquhar (1994). The mean annual isotopic fractionation is estimated by weighting the monthly fractionation of the  $C_3$  and  $C_4$  plants in all PFTs with the respective NPP. The isotopic fractionation is allocated to the output biome and weighted according to the NPP of each PFT (Hatté & Guiot, 2005). The BIOME4 model is particularly useful for simulating paleovegetation because it requires only a limited number of inputs, including monthly temperature, precipitation, sunshine, absolute minimum temperature, atmospheric  $CO_2$  concentration, and soil texture.

### 3.2 Inverse modeling approach

We used a new version of an inverse vegetation model to estimate the climate. The new model inversion (Fig. 4) is a combination of the inverse modeling approaches that are based on pollen-derived biomes (Wu *et al.*, 2007) and  $\delta^{13}\text{C}$  (Hatté & Guiot, 2005). The two inverse methods have been validated in Eurasia and Africa (Wu *et al.*, 2007) and the United States and Australia (Hatté & Guiot, 2005). This integration provides an important advantage for a more complete simulation of the vegetation composition because it can both discriminate among the different types of  $\text{C}_3$  plants (i.e., trees, shrubs, cool season grasses) and reconstruct the portions of the  $\text{C}_3$  and  $\text{C}_4$  plants constrained by the seasonal climate and atmospheric  $\text{CO}_2$  levels. This provides a suitable approach for extracting detailed paleo-seasonality information (i.e., summer rainfall and temperature) and the effect of  $\text{CO}_2$  on ecological succession in the Himalayan foreland since the late Miocene.

The inversion process consists of finding all the combinations of climatic factors that could be compatible with the biome inferred from the pollen in a time period at a given site and the corresponding measured  $\delta^{13}\text{C}$  value (Fig. 4). The main climate variables driving the vegetation in the BIOME4 model are the monthly temperature, precipitation, and sunshine; these are the unknown variables estimated by the model inversion. To limit the number of degrees of freedom, we constrain these unknowns to January and July temperature and precipitation (four variables) and estimate the other monthly variables using empirical equations based on four parameters (Guiot *et al.*, 2000). The monthly temperature and precipitation are deduced by a sinusoidal interpolation between January and July. The sunshine percentage is estimated by a linear regression from the temperature and precipitation of the same month (Guiot *et al.*, 2000).

The procedure (Fig. 4) is summarized as follows: (1) a set of four variable deviations is randomly sampled, and the other monthly components of the climate are calculated using the empirical equations; (2) the deviations are added to the values of the modern climate and applied to the BIOME4 model; (3) a transfer matrix is used to convert the BIOME4 biome to biome scores comparable to the pollen data (Wu *et al.*, 2007); (4) the simulated biome scores are compared to the pollen scores using a Euclidian distance for biome scores, and the simulated and measured  $\delta^{13}\text{C}$  are compared; (5) the climate set is accepted on the condition that the Euclidian distance is not too high (see Wu *et al.*, 2007) and that the difference between the observed and simulated  $\delta^{13}\text{C}$  values is less than 2.0‰ (the  $\delta^{13}\text{C}$  shift during the pedogenesis and fossilization) (i.e., Balesdent *et al.*, 1993; Van Bergen & Poole, 2002; Nguyen Tu *et al.*, 2004; Poole *et al.*, 2004); (6) if the set of climate vectors is accepted, it is used to calculate the *a posteriori* probability distribution of the unknowns; (7) another climate deviation vector is randomly drawn, and the procedure is repeated. This iterative process was complete when we obtained a sufficient number of valid scenarios to calculate the *a posteriori* probability distributions, namely, 200-300 scenarios in 5000 iterations. In the last step, we deduced the mean climate with a confidence percentage using the *a posteriori* probabilities. A complete model description can be found in Guiot *et al.* (2000) and Wu *et al.* (2007). The *a priori* distribution of the input parameters in this study was set to the ranges provided in Table 1.

### **3.3 A sensitivity analysis of the effects of CO<sub>2</sub> on the C<sub>4</sub> expansion**

The inverse modeling method enables us to reconstruct paleoclimates from the late Miocene to the present under various atmospheric CO<sub>2</sub> concentrations and to investigate potential climate and CO<sub>2</sub> changes that could explain the expansion of the C<sub>4</sub> plant distribution. This method

accepts the concept of a multi-equilibrium status between the environmental conditions (i.e., climate, CO<sub>2</sub>) and the vegetation (Guiot *et al.*, 2000).

To identify the dominant factor linking the climate and the CO<sub>2</sub> concentration controlling the expansion of the C<sub>4</sub> plant distribution during the late Miocene, we performed seven sensitivity experiments with CO<sub>2</sub> levels ranging from 200 to 800 ppmv in increments of 100 ppmv. Meanwhile, the climate (temperature and precipitation) was maintained at its respective reconstructed values (Fig. 5). This CO<sub>2</sub> range covers the late Miocene atmospheric CO<sub>2</sub> concentration variations (from approximately 460 ppmv to 200 ppmv, Fig. 3a) (LaRiviere *et al.*, 2012) in addition to the full range from the early Miocene (Pearson & Palmer, 2000; Pagani *et al.*, 2005). Thus, we investigated the potential effects of very large CO<sub>2</sub> changes (*y*-axis direction in Fig. 6) on the observed expansion of the C<sub>4</sub> plants in the Siwalik. Furthermore, because the reconstructed paleoclimate includes all the climate changes since the late Miocene, we can also investigate the climate effects (*x*-axis direction in Fig. 6) on the C<sub>4</sub> expansion by using these experiments with various CO<sub>2</sub> levels.

## 4. Results

### 4.1 Validation of the inverse approach with modern data

We applied the inverse model to modern pollen samples to validate the approach by reconstructing the modern climate at each site and comparing it with the observed values. Because of a shortage of organic  $\delta^{13}\text{C}$  data at the modern pollen sites, we only validated the efficiency of the biome inversion scheme to reproduce the modern climate. This validation was accomplished using the modern pollen biome from China (MCQPD, 2001). The high correlation

This article is protected by copyright. All rights reserved.

coefficients ( $R=0.75-0.95$ ; Table 2), intercepts close to 0 (except for growing degree-days above  $5^{\circ}\text{C}$  and the mean temperature of the warmest month), and slopes close to 1 (except for the July precipitation) demonstrated that the inversion method worked well for most variables in China.

Although we could validate if the approach is improved by using the biome data in addition to the  $\delta^{13}\text{C}$  data, the BIOME4 simulation of the discrimination of carbon isotopes in the leaves has already been validated by Kaplan *et al.* (2002) over the entire range of plant types, including  $\text{C}_4$ . The general reliability of the  $\delta^{13}\text{C}$  inversion to reconstruct the climate was validated by Hatté and Guiot (2005) using modern data from the woodlands along a 900 km-long rainfall gradient in southern Queensland, Australia (Stewart *et al.*, 1995), and from the grasslands and woodlands along two transects in southeastern Utah and south-central New Mexico (United States) (Van de Water *et al.*, 2002), where precipitation ranges from 160 to 1690 mm/year. The correlation coefficient ( $R$ ) was approximately 0.95 ( $y = 0.9711x + 6.3994$ ) between the observed ( $y$ ) and reconstructed precipitation ( $x$ ). The studies indicated that  $\delta^{13}\text{C}$  was particularly efficient for the precipitation signal. In our inversion process,  $\delta^{13}\text{C}$  is a constraint added to pollen proxies. The main effect is to decrease the uncertainties rather than to change the reconstructions. We conclude that the climate signals contained in the pollen and  $\delta^{13}\text{C}$  data can be quantitatively extracted by this method.

#### **4.2 Biome and climate reconstruction since the late Miocene**

During the late Miocene period, a marked shift from  $-25\text{‰}$  to  $-14\text{‰}$  occurred in organic carbon isotope ratios in the Nepal Siwalik (Fig. 2). This shift was accompanied by a shift from the dominantly  $\text{C}_3$  temperate deciduous forest and broadleaved evergreen/warm mixed forest that

This article is protected by copyright. All rights reserved.

existed prior to 7 Myr to the more seasonal water-stressed C<sub>4</sub> grasses of 7 to 5 Myr. By 5 Myr, the C<sub>4</sub> grasses dominated the Siwalik biomass. A similar expansion of the C<sub>4</sub> grasses was observed in other surveys of the Himalayan foothills and the Ganges floodplain (Quade *et al.*, 1989; Cerling *et al.*, 1997).

The inverse vegetation model successfully simulated the biome types at most pollen collection sites (Fig. 2a) and reconstructed the major expansion of the C<sub>4</sub> grass distribution. The expansion was characterized by more positive  $\delta^{13}\text{C}$  values (Fig. 2b) between 12 and 3 Myr. These results indicate that the mean annual temperature, approximately 12 to 13°C, was lower than the modern value prior to 8 Myr; therefore, the temperature increased significantly since 8 Myr (Fig. 5a).

The changes in the ratio of actual to potential evapotranspiration ( $\alpha$ ) present the opposite trend, with values that generally averaged approximately 10% higher than the present before 7 Myr and decreased significantly between 7 and 6.5 Myr, reaching minimum values that were approximately 25% lower than the modern values within the last 5 Myr (Fig. 5b). The annual precipitation pattern (Fig. 5c) is similar to that of  $\alpha$ . The seasonal reconstruction revealed that this annual precipitation shift is mainly attributed to decreases in the summer rainfall, whereas winter rainfall did not change significantly (Fig. 5d).

#### **4.3 The impact of CO<sub>2</sub> concentration on the C<sub>4</sub> expansion**

The results of the seven sensitivity experiments (Fig. 6) with various CO<sub>2</sub> concentrations indicate that the C<sub>4</sub> plant composition responded negatively to changes in CO<sub>2</sub> concentration during all climate changes. More C<sub>4</sub> plants were present at lower CO<sub>2</sub> levels, suggesting that the lower CO<sub>2</sub> levels favored the C<sub>4</sub> plants. The increase of the C<sub>4</sub> plant biomass (Fig. 6a) in response to the

CO<sub>2</sub> level decline was more significant for the higher temperature and lower precipitation observed within the last 8 Myr than for the relatively constant low temperature and high precipitation prior to 8 Myr ago (Fig. 5). These findings suggest that C<sub>4</sub> plants have been favored by a warmer and drier climate. The mean change of C<sub>4</sub> plant biomass was approximately 20% higher (Fig. 6b) when the atmospheric CO<sub>2</sub> concentration decreased from 800 to 200 ppmv, regardless of the climate changes, whereas the C<sub>4</sub> biomass change was approximately 60% higher (Fig. 6b) with the reconstructed warmer and drier climate, regardless of the CO<sub>2</sub> levels. Therefore, the C<sub>4</sub> plants had a weaker response to the atmospheric CO<sub>2</sub> concentration decrease of 600 ppmv than to the climate change reconstructed for the late Miocene.

## 5. Discussion and Conclusions

### 5.1 Climate change during the late Miocene and its relationship with the C<sub>4</sub> distribution

With ecological succession from C<sub>3</sub> temperate deciduous forest and broadleaved evergreen/warm mixed forest to C<sub>4</sub> grasses, our climate reconstruction shows that the mean annual temperature in the Siwalik region increased between 8 and 3 Myr; the highest rate was identified between 8 to 5 Myr. This relationship between the abundance of C<sub>4</sub> and temperature increase is consistent with the modern environmental characteristics in non-arctic environments that favor C<sub>4</sub> plants: more C<sub>4</sub> plants exist during higher annual temperatures (Cavagnaro, 1988; Ueno & Takeda, 1992; Bird & Pousai, 1997; Pyankov *et al.*, 2010). This pattern is particularly prevalent during the higher temperatures of the growing season for the C<sub>4</sub> grasses (Teeri & Stowe, 1976; Hattersley *et al.*, 1983; Collatz *et al.*, 1998; Sage *et al.*, 1999). The occurrence is due to the differences in temperature dependence of the photosynthetic efficiency for CO<sub>2</sub> uptake of C<sub>3</sub> and C<sub>4</sub> plants (Ehleringer *et al.*, 1997). The quantum yield (photosynthetic efficiency) of C<sub>3</sub> plants declines

This article is protected by copyright. All rights reserved.

with increasing temperature, but C<sub>4</sub> plants are not affected. As such, C<sub>4</sub>-dominated ecosystems are favored by high temperatures under reduced CO<sub>2</sub> conditions. The cause of the temperature increase within the last 8 Myr in the Siwalik will be discussed in Section 5.3.

Another observation of our study is that increased aridity 7 Myr ago (Fig. 5b, c) accompanied the expansion of the C<sub>4</sub> grasses in the Siwalik. This correlation between the aridity and the abundance of C<sub>4</sub> in the Siwalik is consistent with evidence from the modern C<sub>4</sub> plant distribution in Europe (Pyankov *et al.*, 2010) and C<sub>4</sub> dicots in North America (Stowe & Teeri, 1978) along moisture gradients (including woody and grass biomes), where C<sub>4</sub> plants are favored by increased aridity. This pattern can be explained by the fact that the physiology of C<sub>4</sub> plants involves higher ratios of photosynthesis to transpiration (water-use efficiency, WUE) than C<sub>3</sub> plants (Berry, 1975). Thus, C<sub>4</sub> plants have a competitive advantage in areas where moisture supply is limited. If modern woody vegetation is factored out and only grasslands of varying moisture characteristics in drier regions are compared, the relationship between C<sub>4</sub> dominance and the precipitation regime is reversed (Paruelo & Lauenroth, 1996; Schulze *et al.*, 1996; Epstein *et al.*, 1997); a greater number of C<sub>4</sub> plants grow in wetter sites because the C<sub>4</sub> plants are favored by the higher temperature accompanied by relatively more precipitation.

The reconstructed annual precipitation was higher prior to 7 Myr and decreased significantly after 7 Myr (Fig. 5c). This change was mainly attributed to summer precipitation decreases (Fig. 5d). Our results agree with previous results. The seasonality of precipitation, as inferred from the annual  $\delta^{18}\text{O}$  profiles in fossilized freshwater bivalve shells and mammal teeth from the Himalayan foreland (Dettman *et al.*, 2001), identified an intense Indian monsoon prior to 7.5

Myr, with higher overall annual precipitation, especially during the summer monsoon. The long-term precipitation trend, in conjunction with the positive  $\delta^{18}\text{O}$  values in the paleosols of the Siwalik from 8 to 6 Myr (Quade *et al.*, 1989, 1995) and the enriched  $\delta\text{D}$  of plant leaf waxes from ODP Site 722 in the Indian Ocean from 10 to 5.5 Myr (Huang *et al.*, 2007), suggests that the period was characterized by a significant increase in aridity in the Himalayan foreland. A gradual drying climate is also apparent from 11 to 6 Myr, as indicated by the decreased thickness of the leaching zones in the Siwalik paleosols (Quade *et al.*, 1995), the decline of chemical weathering in the Himalayas from 10.5 to 3.5 Myr ago (Clift *et al.*, 2008), and the replacement of woodland-adapted fauna by open-habitat mammals in Pakistan, Nepal, and northern India nearly 8 Myr (Barry *et al.*, 1985).

## **5.2 The effect of CO<sub>2</sub> concentration on the C<sub>4</sub> expansion**

Many studies have addressed the influence of various CO<sub>2</sub> concentrations on plant growth (Hunt *et al.*, 1991; Kimball *et al.*, 1993; Curtis & Wang, 1998; Wand *et al.*, 1999; Poorter & Navas, 2003) and physiological effects, including the alteration of the leaf net photosynthetic rates, stomatal conductance, and WUE (Gunderson & Wullschleger, 1994; Woodward & Kelly, 1995; Saxe *et al.*, 1998; Gagen *et al.*, 2011). CO<sub>2</sub> enrichment increases the water-use efficiency (reduces the water use), which contributes to enhanced soil water content and reduced soil-water depletion (Wullschleger & Tschaplinski, 2002). Plants may be more sensitive to CO<sub>2</sub> enrichment at subambient concentrations than at superambient concentrations (Polley *et al.*, 2002). Although the contribution of CO<sub>2</sub> fertilization to plants is uncertain based on currently available data (Norby *et al.*, 2005), Cowling and Field (2003) observed a good fit between the BIOME3 modeled and observed response of LAI to changes in low CO<sub>2</sub> levels. The predictions of NPP

response to the CO<sub>2</sub> effect using the Lund–Postdam–Jena (LPJ) model (Cramer *et al.*, 2001) is also consistent with the experimental evidence (DeLucia *et al.*, 1999; Norby *et al.*, 2002, 2005). Because the treatment of the CO<sub>2</sub> effect in BIOME3 and LPJ is the same as in BIOME4, these comparisons indicate that the BIOME4 model realistically predicts the response to the CO<sub>2</sub> effect.

Our sensitivity experiments (see Section 3.3 for details) (Fig. 6) using various CO<sub>2</sub> concentrations indicate that more C<sub>4</sub> grasses were present at lower CO<sub>2</sub> levels. The results are consistent with the simulations obtained by the quantum yield model (Cerling *et al.*, 1997; Ehleringer *et al.*, 1997) in which the C<sub>4</sub>-dominated grasses are favored under lower CO<sub>2</sub> concentrations relative to the C<sub>3</sub> grasses. The metabolism is attributed to the different responses of C<sub>3</sub> and C<sub>4</sub> plants to changes in CO<sub>2</sub> concentrations. The C<sub>3</sub> plants respond to lower CO<sub>2</sub> concentrations with decreased maximum net photosynthetic rates because of inherent CO<sub>2</sub> substrate limitations and higher photorespiration rates (Farquhar & von Caemmerer, 1982), whereas C<sub>4</sub> plants are less sensitive to CO<sub>2</sub> levels (Ehleringer *et al.*, 1991).

The difference between our BIOME4 approach and the quantum yield model is that the quantum yield of C<sub>3</sub> and C<sub>4</sub> grasses only varies with CO<sub>2</sub> concentration and temperature (Cerling *et al.*, 1997; Ehleringer *et al.*, 1997), whereas the BIOME4 approach considers the above factors coupled with water stress using a water flux model (Haxeltine & Prentice, 1996). Water stress is assumed to reduce photosynthesis through a reduction in canopy conductance. Regional evapotranspiration is calculated as a function of canopy conductance, equilibrium evapotranspiration rate and soil moisture. This scheme (Haxeltine & Prentice, 1996) results in a

coupling of the carbon and water fluxes for the vegetation simulation through canopy conductance, allowing for a simulation of the response of photosynthesis, stomatal conductance, and leaf area to environmental factors, including atmospheric CO<sub>2</sub>, temperature, and precipitation. Although the transport characteristics of stems, including xylem anatomy and sapwood area, soil and leaf water potential, and stomatal conductance (Sperry, 2000), are not considered in detail in the mechanism of water flux, water is considered a primary factor limiting plant growth and productivity (Schulze *et al.*, 1987; Haxeltine & Prentice, 1996); thus, integrating water flux into the model provides insights into how CO<sub>2</sub> concentration, temperature, and water changes may impact C<sub>3</sub> and C<sub>4</sub> plants in different environments. As a result, the model provides a better understanding of the competition between the C<sub>3</sub> and C<sub>4</sub> plants and the consequences for ecological succession.

Further sensitivity analysis revealed that the expansion of the C<sub>4</sub> grass distribution was less responsive to the CO<sub>2</sub> level decrease (from 800 to 200 ppmv) than to the climate changes (Fig. 6). In fact, the reconstructed record of the atmospheric CO<sub>2</sub> concentrations varies only between approximately 460 ppmv and 200 ppmv during the late Miocene period, with an increase of the CO<sub>2</sub> concentration 5.5 Myr ago (Fig. 3a). The CO<sub>2</sub> changes are only approximately half of the simulated change. Therefore, the effect of climatic change on the expansion of the C<sub>4</sub> plants may be even greater (Fig. 6b) than that produced by the CO<sub>2</sub>. Furthermore, according to the sensitivity analysis (Fig. 6), the CO<sub>2</sub> decrease from 800 to 200 ppmv (y-axis direction in Fig. 6a) was not a sufficient driver by itself to allow the C<sub>4</sub> grasses to dominate (>50% of the total biomass) in the landscape during the late Miocene (prior to 7 Myr). These experiments demonstrate that climate change exerted a greater control over the relative abundances of the C<sub>3</sub>

and C<sub>4</sub> plants than did the CO<sub>2</sub> concentration decrease. Thus, the late Miocene expansion of the C<sub>4</sub> plants in the Siwalik region was not primarily a response to the declining atmospheric CO<sub>2</sub> levels, even if low atmospheric CO<sub>2</sub> was a significant contributing factor to the appearance of C<sub>4</sub> plants (Sage, 2004). Our results agree with the previous findings (Quade *et al.*, 1995; Pagani *et al.*, 1999; Fox & Koch, 2003, 2004; Huang *et al.*, 2007; Strömberg & McInerney, 2011) that the C<sub>4</sub> plant expansion was unlikely driven by atmospheric CO<sub>2</sub> alone.

### 5.3 A possible cause for the expansion of the C<sub>4</sub> plants

An important result of this study is that the mean annual temperature in the Siwalik increased by approximately 12 to 13°C within the last 8 Myr. There are two scales of changes: one global and the other local. Both scales likely contributed to these temperature changes. Generally, local temperature variations are consistent with global changes at a tectonic time scale, but the temperature increase in the Siwalik region differed from the overall global declining temperature trend since the Miocene based on deep-sea oxygen isotope ( $\delta^{18}\text{O}$ ) records (Zachos *et al.*, 2001). This pattern suggests that the Siwalik temperature change cannot be primarily attributed to global factors. Local factors may also have been responsible for the increasing temperature, caused by a decrease in the mean elevation of the Siwalik basin in Nepal, which suggests the existence of a higher elevation prior to 8 Myr ago. This interpretation is consistent with the bulk of the thermochronological evidence (Coleman & Hodges, 1995) with geochemical (Galy *et al.*, 2010), paleoclimatology, and paleovegetation (Garziona *et al.*, 2000; Spicer *et al.*, 2003) studies. This evidence supports the assertion that the Himalayas and the Tibetan Plateau attained higher elevations over large areas prior to 8 Myr ago.

Marine paleo-temperature records (Zachos *et al.*, 2001; Huang *et al.*, 2007) suggest that the global temperature has decreased approximately 2 to 3°C since the late Miocene. Because the reconstructed temperature (approximately 12 to 13°C increase) in the Nepal Siwalik was superimpose both the global and local temperature changes, the local temperature increase was approximately 14 to 16°C within the last 8 Myr. Assuming that this temperature increase corresponds to a decrease in the elevation, given an environmental lapse rate of 6 to 6.5°C km<sup>-1</sup> (Rind & Peteet, 1985), our results suggest a decrease in the elevation of approximately 2200 m. This significant elevation change is in broad agreement with a decrease in the mean watershed elevation of 1000 to 1500 m in the Zada basin, southwestern Tibet, based on oxygen isotope-based paleoelevation reconstructions (Murphy *et al.*, 2009; Saylor *et al.*, 2009).

Most areas of the Siwalik between Pakistan and Nepal recorded an acceleration in the sedimentation nearly 11 Myr and experienced a decline nearly 8 Myr (Burband *et al.*, 1993), indicating a decreasing erosion rate since the late Miocene in this region. Because the sediment flux was attributed to climate change and tectonic activity, this increase in the sediment flux to the Himalayan foreland basin was most likely due to the combined activities of intensified monsoonal precipitation (Dettman *et al.*, 2001) and tectonics (Burband *et al.*, 1996). Thus, the decline in the sediment flux was most likely related to reduced monsoonal precipitation (Dettman *et al.*, 2001) and tectonic activity (Burband *et al.*, 1993). In this context, our climate reconstruction supports the changes in monsoonal precipitation. We suggest that the decrease in the mean Siwalik basin elevation can be explained by significant erosion (based on sediment flux) in the Himalayas (Raymo & Ruddiman, 1992; Rea, 1992; Burband *et al.*, 1993) and tectonic processes (Burband *et al.*, 1993, 1996) since the late Miocene.

The expansion of the C<sub>4</sub> plant distribution in the Himalayan forelands was originally believed to result from the initiation or intensification of the Indian monsoon (Quade *et al.*, 1989). This interpretation is supported by significant increases in the abundance of marine organisms such as *Globigerina bulloides* 8.5 Myr ago, which indicate a stronger monsoon-driven upwelling in the Arabian Sea (Kroon *et al.*, 1991). However, recent studies have revealed contradictory evidence related to biomarker abundance: alkenone UK<sup>37</sup> and *Globigerina bulloides* abundance data from the Bengal Fan (Huang *et al.*, 2007) versus chemical weathering (Clift *et al.*, 2008) and seasonal  $\delta^{18}\text{O}$  variations (Dettman *et al.*, 2001; Garzzone *et al.*, 2000) in the Himalayas do not suggest an enhanced summer monsoon circulation during this period. Furthermore, the apparent diachronous (3 Myr) nature of the C<sub>4</sub> plant distribution expansion in various locations of the Himalayan Siwalik (Sanyal *et al.*, 2010) indicates the importance of the regional climate in controlling the distribution of the C<sub>4</sub> plants, as opposed to the role of the Indian monsoon. If the monsoon were dominant, then it would lead to synchronous C<sub>4</sub> expansion following the changes in the Indian monsoon region. Our results indicate that the relative abundance of C<sub>4</sub> versus C<sub>3</sub> plants in the Nepal Siwalik was mainly controlled by decreased precipitation (especially summer rainfall) and increased temperatures rather than the strengthening of the Indian summer monsoon.

The precipitation decrease during the late Miocene may have resulted, in part, from the northward motion of the Indian plate, which carried the Himalayas to the north of the Intertropical Convergence Zone (ITCZ) (Armstrong & Allen, 2011), or the global trend toward a cooler late Cenozoic climate (LaRiviere *et al.*, 2012), which reduced water vapor in the atmosphere. However, the combination of decreased precipitation and increased temperature

Accepted Article

indicates that this change was at least partly a response to the altitude decline in the Nepal Siwalik. Because the rainfall distribution in the front of the central Himalaya exhibits two amplitude peaks along bands with a mean elevation of  $900\pm 400$  m (the southern margin of the Lesser Himalayas) and  $2100\pm 300$  m (the southern flank of the Greater Himalayas) due to orographic effects (Bookhagen & Burbank, 2006), the pattern of the precipitation decrease in the Siwalik region since 7 Myr is compatible with a sharp reduction of rainfall due to the altitude decrease from the upper peak (our reconstructed paleoaltitude was approximately 2600 m based on adding the decrease of approximately 2200 m to the modern elevation of approximately 400 m in the Nepal Siwalik).

Although our results suggest that the expansion of the C<sub>4</sub> plants in the Nepal Siwalik was triggered primarily by major changes in aridity and temperature that resulted from decreased elevation of the Himalayan foreland and was perhaps amplified by a low atmospheric CO<sub>2</sub> concentration, we cannot rule out other factors for different regions. In the Great Plains of North America, major factors in the C<sub>3</sub> and C<sub>4</sub> shifts might include global cooling (Fox & Koch, 2003, 2004), climatic drying (Strömberg & McInerney, 2011), grass-grazer coevolution (Retallack, 2007), or intensified fire regimes (Keeley & Rundel, 2005). Regional ecological and climatic factors, forced by global climate change (Zachos *et al.*, 2001), are the most likely factors that control the development of C<sub>4</sub> plants in various regions during the late Miocene. Future investigations should consider these changes at the global scale to provide additional evidence for the relative importance of these factors regarding C<sub>4</sub> expansion on different continents.

## Acknowledgments

This research was supported by the Bairen Programs of the Chinese Academy of Sciences (CAS), the National Basic Research Program of China (973 Program, grant no. 2010CB950204), the National Natural Science Foundation of China (grants no. 41125011 and 41071055), and the National Science and Engineering Research Council of Canada (NSERC) discovery grant. This paper is a contribution to OSU-Institut Pytheas and to the Fédération de Recherche ECCOREV.

We thank the anonymous reviewers and Guangsheng Zhuang for their valuable suggestions and comments on the manuscript.

## References:

- Armstrong HA, Allen MB (2011) Shifts in the Intertropical Convergence Zone, Himalayan exhumation, and late Cenozoic climate. *Geology*, **39**, 11-14.
- Balesdent J, Girardin C, Mariotti A (1993) Site-related  $^{13}\text{C}$  of tree leaves and soil organic matter in a temperate forest. *Ecology*, **74**, 1713-1721.
- Barry JC, Johnson NM, Raza SM, Jacobs LL (1985) Neogene mammalian faunal change in southern Asia: correlations with climatic, tectonic, and eustatic events. *Geology*, **13**, 637-640.
- Bartoli G, Hönisch B, Zeebe R (2011) Atmospheric  $\text{CO}_2$  decline during the Pliocene intensification of Northern Hemisphere Glaciations. *Paleoceanography*, **26**, PA4213.
- Beerling DJ, Fox A, Anderson CW (2009) Quantitative uncertainty analyses of ancient atmospheric  $\text{CO}_2$  estimates from fossil leaves. *American Journal of Science*, **309**, 775-787.
- Bender MM (1971) Variations in the  $^{13}\text{C}/^{12}\text{C}$  ratios of plants in relation to the pathway of photosynthetic carbon dioxide fixation. *Phytochemistry*. **10**, 1239-1245.
- Berry JA (1975) Adaptation of Photosynthetic Processes to Stress. *Science*, **188**, 644-650.

- Bird M, Pousai P (1997) Variations of  $\delta^{13}\text{C}$  in the surface soil organic carbon pool. *Global Biogeochemistry Cycles*, **11**, 313-322.
- Bookhagen B, Burbank DW (2006) Topography, relief, and TRMM-derived rainfall variations along the Himalaya. *Geophysical Research Letters*, **33**, L08405.
- Boom A, Marchant R, Hooghiemstra H, Sinninghe Damsté JS (2002)  $\text{CO}_2$ - and temperature-controlled altitudinal shifts of  $\text{C}_4$ - and  $\text{C}_3$ -dominated grasslands allow reconstruction of palaeoatmospheric  $p\text{CO}_2$ . *Palaeogeography, Palaeoclimatology, Palaeoecology*, **177**, 151-168.
- Burbank DW, Derry LA, France-Lanord C (1993) Reduced Himalayan sediment production 8 Myr ago despite an intensified monsoon. *Nature*, **346**, 48-50.
- Burbank DW, Beck AR, Mulder T (1996) The Himalayan foreland basin. In: The Tectonic Evolution of Asia (eds Yin A, Harrison M), pp. 149-188, Cambridge University Press, USA.
- Cande SC, Kent DV (1995) Revised calibration of the geomagnetic polarity timescale for the Late Cretaceous and Cenozoic. *Journal of Geophysical Research*, **100**, 6093-6095.
- Cavagnaro JB (1988) Distribution of  $\text{C}_3$  and  $\text{C}_4$  grasses at different altitudes in a temperate arid region of Argentina. *Oecologia*, **76**, 273-277.
- Cerling TE, Harris JM, MacFadden BJ, Leakey MG, Quadek J, Eisenmann V, Ehleringer JR (1997) Global vegetation change through the Miocene and Pliocene. *Nature*, **389**, 153-158.
- Clift PD, Hodges KV, Heslop D, Hannigan R, Van Long H, Calves G (2008) Correlation of Himalayan exhumation rates and Asian monsoon intensity. *Nature Geoscience*, **1**, 875-880.
- Coleman M, Hodges K (1995) Evidence for Tibetan plateau uplift before 14 Myr ago from a new minimum age for east-west extension. *Nature*, **374**, 49-51.
- Collatz G, Berry J, Clark J (1998) Effects of climate and atmospheric  $\text{CO}_2$  partial pressure on the

global distribution of C<sub>4</sub> grasses: Present, past, and future. *Oecologia*, **114**, 441-454.

Cowling SA, Field CB (2003) Environmental control of leaf area production: implications for vegetation and land-surface modeling. *Global Biogeochemistry Cycle*, **17**, 1007, doi:10.1029/2002GB001915.

Cramer W, Bondeau A, Woodward FI, Prentice IC, Betts RA, Brovkin V, Cox PM, Fisher V, Foley JA, Friend AD, Kucharik C, Lomas M, Ramankutty N, Sitch S, Smith B, White A, Young-Molling C (2001) Global response of terrestrial ecosystem structure and function to CO<sub>2</sub> and climate change: Results from six dynamic global vegetation models. *Global Change Biology*, **7**, 357-373.

Curtis PS, Wang X (1998) A meta-analysis of elevated CO<sub>2</sub> effects on woody plant mass, form, and physiology. *Oecologia*, **113**, 299-313.

Dettman DL, Kohn MJ, Quade J, Ryerson FJ, Ojha TP, Hamidullah S (2001) Seasonal stable isotope evidence for a strong Asian monsoon throughout the past 10.7 m.y. *Geology*, **29**, 31-34.

Edwards EJ, Still CJ (2008) Climate, phylogeny and the ecological distribution of C<sub>4</sub> grasses. *Ecology Letter*, **11**, 266-276.

Ehleringer JR, Cerling TE, Helliker BR (1997) C<sub>4</sub> photosynthesis, atmospheric CO<sub>2</sub>, and climate. *Oecologia*, **112**, 285-299.

Ehleringer JR, Sage RF, Flanagan LB, Pearcy RW (1991) Climate change and the evolution of C<sub>4</sub> photosynthesis. *Trends in Ecology & Evolution*, **6**, 95-99.

Epstein HE, Lauenroth WK, Burke IC, Coffin DP (1997) Productivity patterns of C<sub>3</sub> and C<sub>4</sub> functional types in the U.S. Great Plains. *Ecology*, **78**, 722-731.

Farquhar GD, von Caemmerer S (1982) Modeling of photosynthetic response to environmental

conditions. *Encyclopedia of Plant Physiology*, **12**, 549-587.

Farquhar GD (1983) On the nature of carbon isotope discrimination in C<sub>4</sub> species. *Australian Journal of Plant Physiology*, **10**, 205-226.

Food and Agriculture Organization (FAO) (1995) *Digital Soil Map of the World and Derived Soil Properties*. Food and Agriculture Organization, Rome.

Fox DL, Koch PL (2003) Tertiary history of C<sub>4</sub> biomass in the Great Plains, USA. *Geology*. **31**, 809-812.

Fox DL, Koch PL (2004) Carbon and oxygen isotopic variability in Neogene paleosol carbonates: constraints on the evolution of the C<sub>4</sub>-grasslands of the Great Plains, USA. *Palaeogeography, Palaeoclimatology, Palaeoecology*. **207**, 305-329.

Gagen M, Finsinger W, Wagner-Cremer F, McCarroll D, Loader NJ, Robertson I, Jalkanen R, Young G, Kirchhefer A (2011) Evidence of changing intrinsic water-use efficiency under rising atmospheric CO<sub>2</sub> concentrations in Boreal Fennoscandia from subfossil leaves and tree ring  $\delta^{13}\text{C}$  ratios. *Global Change Biology*. **17**, 1064-1072.

Galy V, France-Lanord C, Peucker-Ehrenbrink B, Huyghe P (2010) Sr–Nd–Os evidence for a stable erosion regime in the Himalaya during the past 12 Myr. *Earth and Planetary Science Letters*, **290**, 474-480.

Garzione CN, Dettman DL, Quade J, DeCelles PG, Butler RF (2000) High times on the Tibetan Plateau: paleoelevation of the Thakkhola graben, Nepal. *Geology*, **28**, 339-342.

Guiot J, Cheddadi R, Prentice IC, Jolly D (1996) A method of biome and land surface mapping from pollen data: application to Europe 6000 years ago. *Palaeoclimates: Data Model*, **1**, 311-324.

Guiot J, Goeury C (1996) PPPBASE, a software for statistical analysis of paleoecological and

paleoclimatological data. *Dendrochronologia*, **14**, 295-300.

Guiot J, Torre F, Jolly D, Peyron O, Boreux JJ, Cheddadi R (2000) Inverse vegetation modeling by Monte Carlo sampling to reconstruct palaeoclimate under changed precipitation seasonality and CO<sub>2</sub> conditions: application to glacial climate in Mediterranean region.

*Ecology Modelling*, **127**, 119-140.

Gunderson CA, Wullschleger SD (1994) Photosynthetic acclimation in trees to rising atmospheric CO<sub>2</sub>: a broader perspective. *Photosynthesis Research*, **39**, 369-388.

Harrison SP, Prentice C (2003) Climate and CO<sub>2</sub> controls on global vegetation distribution at the last glacial maximum: analysis based on palaeovegetation data, biome modelling and palaeoclimate simulations. *Global Change Biology*, **9**, 983-1004.

Hatté C, Guiot J (2005) Palaeoprecipitation reconstruction by inverse modelling using the isotopic signal of loess organic matter: application to the Nußloch loess sequence (Rhine Valley, Germany). *Climate Dynamics*, **25**, 315-327.

Hattersley PW (1983) The distribution of C<sub>3</sub> and C<sub>4</sub> grasses in Australia in relation to climate. *Oecologia*, **57**, 113-128.

Hattersley PW (1983) The distribution of C<sub>3</sub> and C<sub>4</sub> grasses in Australia in relation to climate. *Oecologia*, **57**, 113-128.

Haxeltine A, Prentice IC (1996) BIOME3: An equilibrium terrestrial biosphere model based on ecophysiological constraints, resource availability and competition among plant functional types, *Global Biogeochemistry Cycle*, **10**, 693-709.

Higgins SI, Simon S (2012) Atmospheric CO<sub>2</sub> forces abrupt vegetation shifts locally, but not globally. *Nature*, **488**, 209-212.

Hönisch B, Hemming NG, Archer D, Siddall M, McManus JF (2009) Atmospheric carbon

dioxide concentration across the Mid-Pleistocene Transition. *Science*, **324**, 1551-1554.

Hoorn C, Ohja T, Quade J (2000) Palynological evidence for vegetation development and climatic change in the Sub-Himalayan Zone (Neogene, Central Nepal). *Palaeogeography, Palaeoclimatology, Palaeoecology*, **163**, 133-161.

Huang YS, Clemens SC, Liu WG, Wang Y, Prell WL (2007) Large-scale hydrological change drove the late Miocene C<sub>4</sub> plant expansion in the Himalayan foreland and Arabian Peninsula. *Geology*, **35**, 531-534.

Hunt R, Hand DW, Hannah MA, Neal AM (1991) Response to CO<sub>2</sub> enrichment in 27 herbaceous species. *Functional Ecology*, **5**, 410-421.

Jolly D, Haxeltine A (1997) Effect of low glacial atmospheric CO<sub>2</sub> on tropical African montane vegetation. *Science*, **276**, 786-788.

Kaplan JO, Bigelow NH, Prentice IC *et al.* (2003) Climate change and arctic ecosystems: 2. Modeling, paleodata-model comparisons, and future projections. *Journal of Geophysical Research*, **108**, 8171, doi: 10.1029/2002JD002559.

Kaplan JO, Prentice IC, Buchmann N (2002) The stable carbon isotope composition of the terrestrial biosphere: Modeling at scales from the leaf to the globe. *Global Biogeochemical Cycles*, **16**, 1060, doi:10.1029/2001GB001403.

Keeley JE, Rundel PW (2005) Fire and the Miocene expansion of C<sub>4</sub> grasslands. *Ecology Letter*, **8**, 683-690.

Kimball BA, Mauney JR, Nakamura H, Idso SB (1993) Effects of increasing atmospheric CO<sub>2</sub> on vegetation. *Vegetatio*, **104**, 65-75.

Kroon D, Steens T, Troelstra SR (1991) Onset of monsoonal related upwelling in the western Arabian Sea as revealed by planktonic foraminifers. *Proceedings of the Ocean Drilling*

*Program - Scientific Results*, **117**, 257-263.

- Kürschner WM, Kvacek Z (2009) Oligocene-Miocene CO<sub>2</sub> fluctuations, climatic and palaeofloristic trends inferred from fossil plant assemblages in central Europe. *Bulletin of Geosciences*, **84**, 189-202.
- Kürschner WM, Van Der Burgh J, Visscher H, Dilcher DL (1996) Oak leaves as biosensors of late Neogene and early Pleistocene paleoatmospheric CO<sub>2</sub> concentrations. *Marine Micropaleontology*, **27**, 299-312.
- LaRiviere JP, Ravelo AC, Crimmins A, Dekens PS, Ford HL, Lyle M, Wara MW (2012) Late Miocene decoupling of oceanic warmth and atmospheric carbon dioxide forcing. *Nature*, **486**, 97-100.
- Lloyd J, Farquhar GD (1994) <sup>13</sup>C discrimination during CO<sub>2</sub> assimilation by the terrestrial biosphere. *Oecologia*, **99**, 201-215.
- Members of China Quaternary Pollen Database (MCQPD) (2001) Simulation of China biome reconstruction based on pollen data from surface sediment samples. *Journal of Integrative Plant Biology*, **43**, 201-209.
- Murphy MA, Saylor JE, Ding L (2009) Late Miocene topographic inversion in southwest Tibet based on integrated paleoelevation reconstructions and structural history. *Earth and Planetary Science Letters*, **282**, 1-9.
- New M, Lister D, Hulme M, Makin I (2000) A high-resolution data set of surface climate over global land areas. *Climate Research*, **21**, 1-25.
- Nguyen Tu TT, Derenne S, Largeau C, Bardoux G, Mariotti A (2004) Diagenesis effects on specific carbon isotope composition of plant n-alkanes. *Organic Geochemistry*, **35**, 317-329.
- Norby RJ, DeLucia EH, Gielen B, Calfapietra C, Giardina CP, King JS, Ledford J, McCarthy HR,

Moore DJP, Ceulemans R, Angelis PD, Finzi AC, Karnosky DF, Kubiske ME, Lukac M, Pregitzer KS, Scarascia-Mugnozza GE, Schlesinger WH, Oren R (2005) Forest response to elevated CO<sub>2</sub> is considered across a broad range of productivity. *Proceedings of the National Academy of Sciences of the United States of America*, **102**, 18052-18056.

Norby RJ, Hanson PJ, O'Neill EG, Tschaplinski TJ, Weltzin JF, Hansen RA, Cheng WX, Wullschleger SD, Gunderson CA, Edwards NT, Johnson DW (2002) Net primary productivity of a CO<sub>2</sub>-enriched deciduous forest and the implications for carbon storage. *Ecological Applications*, **12**, 1261-1266.

Pagani M, Freeman KH, Arthur MA (1999) Late Miocene atmospheric CO<sub>2</sub> concentrations and the expansion of C<sub>4</sub> Grasses. *Science*, **285**, 876-879.

Pagani M, Liu ZH, LaRiviere J, Ravelo AC (2010) High Earth-system climate sensitivity determined from Pliocene carbon dioxide concentrations. *Nature Geoscience*, **3**, 27-30.

Pagani M, Zachos J, Freeman KH, Tipple BJ, Bohaty S (2005) Marked change in atmospheric carbon dioxide concentrations during the Oligocene. *Science*, **309**, 600-603.

Paruelo JM, Lauenroth WK (1996) Relative abundance of plant functional types in grasslands and shrublands of North America. *Ecological Applications*, **6**, 1212-1224.

Passey BH, Cerling TE, Perkins ME, Voorhies MR, Harris JM, Tucker ST (2002) Environmental change in the Great Plains: An isotopic record from fossil horses. *Journal of Geology*, **110**, 123-140.

Pearson PN, Palmer MR (2000) Atmospheric carbon dioxide concentrations over the past 60 million years. *Nature*, **406**, 695-699.

Polley HW, Johnson HB, Derner JD (2002) Soil- and plant-water dynamics in a C<sub>3</sub>/C<sub>4</sub> grassland exposed to a subambient to superambient CO<sub>2</sub> gradient. *Global Change Biology*, **8**,

1118-1129.

Poole I, van Bergen PF, Kool J, Schouten S, Cantrill DJ (2004) Molecular isotopic heterogeneity of fossil organic matter: implications for  $^{13}\text{C}$  biomass and  $^{13}\text{C}$  palaeoatmosphere proxies.

*Organic Chemistry*, **35**, 1261-1274.

Poorter H, Navas ML (2003) Plant growth and competition at elevated  $\text{CO}_2$ : on winners, losers and functional groups. *New Phytology*, **157**, 175-198.

Pyankov VI, Ziegler H, Akhan H, Deigele C, Luttge U (2010) European plants with  $\text{C}_4$  photosynthesis: geographical and taxonomic distribution and relations to climate parameters.

*Botanical Journal of the Linnean Society*, **163**, 283-304.

Quade J, Cater JML, Ojha TP, Adam J, Harrison TM (1995) Late Miocene environmental change in Nepal and the northern Indian subcontinent: stable isotopic evidence from palaeosols.

*Geological Society of America Bulletin*, **107**, 1381-1397.

Quade J, Cerling TE, Bowman JR (1989) Development of Asian monsoon revealed by marked ecological shift during the latest Miocene in northern Pakistan. *Nature*, **342**, 163-166.

Raymo ME, Ruddiman WF (1992) Tectonic forcing of late Cenozoic climate. *Nature*, **359**, 117-122.

Rea DK (1992) Delivery of Himalayan sediment to the northern Indian Ocean and its relation to global climate, sea level, uplift, and seawater strontium. In: *Synthesis of results from scientific drilling in the Indian Ocean* (eds Duncan R, *et al.*), vol. 70, pp. 387-402, American Geophysical Union, Geophysical Monograph.

Retallack GJ (2007) Cenozoic paleoclimate on land in North America. *Journal of Geology*. **115**, 271-294.

Rind D, Peteet D (1985) Terrestrial conditions at the last glacial maximum and CLIMP

sea-surface temperature estimates: are they consistent? *Quaternary Research*, **24**, 1-22.

Sage RF (2004) The evolution of C<sub>4</sub> photosynthesis. *New Phytologist*, **161**, 341-170.

Sage RF, Wedin DA, Li MR (1999) The biogeography of C<sub>4</sub> photosynthesis: patterns and controlling factors. In: *C<sub>4</sub> Plant Biology* (eds Sage RF, Monson RK), pp. 313-376, Academic Press, San Diego, California, USA.

Sanyal P, Sarkara A, Bhattacharyab SK, Kumarc R, Ghoshc SK, Agrawala S (2010)

Intensification of monsoon, microclimate and asynchronous C<sub>4</sub> appearance: Isotopic evidence from the Indian Siwalik sediments. *Palaeogeography, Palaeoclimatology, Palaeoecology*, **296**, 165-173.

Savin SM, Hodell D, Kennett JP, Murphy M, Keller G, Killingley J, Vincent E (1985) The evolution of Miocene surface and near-surface marine temperatures: Oxygen isotopic evidence. *Geological Society of America Memoirs*. **163**, 49-73.

Saxe H, Ellsworth DS, Heath J (1998) Tree and forest functioning in an enriched CO<sub>2</sub> atmosphere. *New Phytologist*, **139**, 395-436.

Saylor JE, Quade J, Dettman DL, DeCelles PG, Kapp PA, Ding L (2009) The Late Miocene through present paleoelevation history of southwestern Tibet. *American Journal of Science*, **309**, 1-42.

Schulze ED, Ellis R, Schulze W, Trimborn P, Ziegler H (1996) Diversity, metabolic types and  $\delta^{13}\text{C}$  carbon isotope ratios in the grass flora of Namibia in relation to growth form, precipitation and habitat conditions. *Oecologia*, **106**, 352-369.

Schulze ED, Robichaux RH, Grace J, Rundel PW, Ehleringer JR (1987) Plant water balance. *Bioscience*, **37**, 30-37.

Seki O, Fosterc GL, Schmidtd DN, Mackensene A, Kawamurab K, Pancosta RD (2010)

Alkenone and boron-based Pliocene  $p\text{CO}_2$  records. *Earth and Planetary Science Letters*, **292**, 201-211.

Spangler WML, Jenne RL (1988) *World monthly surface station climatology*. NCAR, Scientific Computing Division, Report. 6 p + CD-ROM.

Sperry JS (2000) Hydraulic constraints on plant gas exchange. *Agricultural and Forest Meteorology*, **104**, 13-23.

Spicer RA, Harris NB, Widdowson M, Herman AB, Guo S, Valdes PJ, Wolfe JA, Kelley SP (2003) Constant elevation of southern Tibet over the past 15 million years. *Nature*, **421**, 622-624.

Stewart GR, Turnbull MH, Schmidt S, Reskine PD (1995)  $^{13}\text{C}$  natural abundance in plant communities along a rainfall gradient: a biological integrator of water availability. *Australian Journal of Plant Physiology*, **22**, 51-55.

Stowe LG, Teeri JA (1978) The geographic distribution of  $\text{C}_4$  species of the Dicotyledonae in relation to climate. *The American Naturalist*, **112**, 609-623.

Strömberg CAE, McInerney FA (2011) The Neogene transition from  $\text{C}_3$  to  $\text{C}_4$  grasslands in North America: assemblage analysis of fossil phytoliths. *Paleobiology*, **37**, 50-71.

Stults DZ, Wagner-Cremer F, Axsmith BJ (2011) Atmospheric paleo- $\text{CO}_2$  estimates based on *Taxodium distichum* (Cupressaceae) fossils from the Miocene and Pliocene of Eastern North America. *Palaeogeography, Palaeoclimatology, Palaeoecology*, **309**, 327-332.

Teeri JA, Stowe LG (1976) Climatic patterns and the distribution of  $\text{C}_4$  grasses in North America. *Oecologia*, **23**, 1-12.

Tipple BJ, Pagani M (2007) The early origins of terrestrial  $\text{C}_4$  photosynthesis. *Annual Review of Earth and Planetary Sciences*, **35**, 435-461.

- Ueno O, Takeda T (1992) Photosynthetic pathway types, ecological characteristics, and geographical distribution of the Cyperaceae in Japan. *Oecologia*, **89**, 195-203.
- van Bergen PF, Poole I (2002) Stable carbon isotopes wood: a clue of palaeoclimate? *Palaeogeography, Palaeoclimatology, Palaeoecology*, **182**, 31-45.
- Van de Water PK, Leavitt SW, Betancourt JL (2002) Leaf  $\delta^{13}\text{C}$  variability with elevation, slope aspect, and precipitation in the southwest United States. *Oecologia*, **132**, 332-343.
- Van Der Burgh J, Visscher H, Dilcher DL, Kürschner WM (1993) Paleoatmospheric signatures in Neogene fossil leaves. *Science*, **260**, 1788-1790.
- Wand SJE, Midgley GF, Jones MH, Curtis PS (1999) Responses of wild  $\text{C}_4$  and  $\text{C}_3$  grass (Poaceae) species to elevated atmospheric  $\text{CO}_2$  concentration: a meta-analytic test of current theories and perceptions. *Global Change Biology*, **5**, 723-741.
- Woodward FI, Kelly CK (1995) The influence of  $\text{CO}_2$  concentration on stomatal density. *New Phytologist*, **131**, 311-327.
- Wu HB, Guiot J, Brewer S, Guo ZT (2007) Climatic changes in Eurasia and Africa at the Last Glacial Maximum and the mid-Holocene: reconstruction from pollen data using inverse vegetation modelling. *Climate Dynamics*, **29**, 211-229.
- Wu HB, Guiot J, Brewer S, Guo ZT, Peng CH (2007) Dominant factors controlling glacial and interglacial variations in the treeline elevation in tropical Africa. *Proceedings of the National Academy of Sciences of the United States of America*, **104**, 9720-9724.
- Wullschleger SD, Tschaplinski TJ, Norby RJ (2002) Plant water relations at elevated  $\text{CO}_2$ -implications for water-limited environments. *Plant, Cell and Environment*, **25**, 319-331.
- Zachos J, Pagani M, Sloan L, Thomas E, Billups K (2001) Trends, rhythms, and aberrations in global climate 65 Ma to present. *Science*, **292**, 686-693.

Zhang CF, Wang Y, Deng T, Wang XM, Biasatti D, Xu YF, Li Q (2009) C<sub>4</sub> expansion in the central Inner Mongolia during the latest Miocene and early Pliocene. *Earth and Planetary Science Letters*, **287**, 311-319.

### Figure Legends

**Figure 1.** Location of the Surai Khola region in Nepal. RT: Ramgarh thrust; MCT: main central thrust; MBT: main boundary thrust; MFT: main frontal thrust.

**Figure 2.** The vegetation and carbon isotope changes in the Surai Khola region of the Siwalik of Nepal. (a) The biomes reconstructed from the pollen samples and biomes simulated using an inverse vegetation model. A pollen sample is assigned to the biome with which it has the maximum affinity, and only the dominant biome scores are plotted in the figure. Biome types: WAMF: broadleaved evergreen/warm mixed forest; TEDE: temperate deciduous forest; TRFO: tropical rain forest; TSFO: tropical seasonal forest; COMX: cool mixed forest; STEP: steppe. (b) The observed and simulated carbon isotope values. The error bars represent 99% confidence intervals. The biome and carbon isotope data from the pollen sites were not successfully simulated by the inverse model more recently than 3 Myr ago because the carbon isotope values were too positive to be simulated. Thus, we only considered the time between 12 and 3 Myr ago, a period contained in both records.

**Figure 3.** The atmospheric CO<sub>2</sub> concentration and carbon isotopic composition since the late Miocene. (a) The atmospheric CO<sub>2</sub> concentration. (b) The atmospheric CO<sub>2</sub> δ<sup>13</sup>C. The estimates of CO<sub>2</sub> concentration from boron isotopes (Hönisch *et al.*, 2009; Seki *et al.*, 2010; Bartoli *et al.*, 2011), plant stomata (Van Der Burgh *et al.*, 1993; Kürschner *et al.*, 1996; Beerling *et al.*, 2009; Kürschner & Kvacek, 2009; Stults *et al.*, 2011), and alkenones (Pagani *et al.*, 1999, 2010; Seki *et*

*al.*, 2010). Estimates of atmospheric CO<sub>2</sub> δ<sup>13</sup>C based on the δ<sup>13</sup>C of planktonic foraminifera calcite (Passey *et al.*, 2002). The error bars represent the reported uncertainty in the estimates.

**Figure 4.** A schematic diagram of the inverse vegetation modeling approach for the paleoclimatic reconstruction. The detailed procedure is described in the methodology (Section 3.2).

**Figure 5.** Reconstruction of the climate anomalies (expressed as deviations from the present value) since the late Miocene in the Siwalik by means of inverse modeling. (a) The mean annual temperature. (b) The ratio of the actual to potential evapotranspiration ( $\alpha$ ). (c) The mean annual precipitation. (d) Summer (June, July, and August) and winter (December, January, and February) precipitation. The mean annual temperature is approximately 24.3°C, and the mean annual precipitation is approximately 1612 mm in Surai Kholā at the present time. The values are means, and the error bars represent the 99% confidence intervals.

**Figure 6.** Sensitivity analysis of the response of the expansion of the C<sub>4</sub> plants in the Siwalik region to changes in the atmospheric CO<sub>2</sub> concentration (*y*-axis direction) and climate (*x*-axis direction) since the late Miocene. (a) The percentage of the C<sub>4</sub> plant biomass (% of the total). The reconstruction of the C<sub>4</sub> plant biomass is based on differences in the C<sub>3</sub> and C<sub>4</sub> plant end-member δ<sup>13</sup>C values with changes in the climate, atmospheric CO<sub>2</sub> level, and δ<sup>13</sup>C<sub>CO2</sub> using the BIOME4 approach. As a result, this reconstruction is more accurate than those that assume δ<sup>13</sup>C end-members are constant. (b) Box plots of the changes in the C<sub>4</sub> plant biomass from the effects of the atmospheric CO<sub>2</sub> concentration (200 to 800 ppmv and 200 to 500 ppmv) and climate. The boxes indicate the interquartile intervals (25th and 75th percentiles), and the bars represent 90% intervals (5th and 95th percentiles). (c) Changes in the organic carbon isotopic

composition. The observed values are the  $\delta^{13}\text{C}$  of the five-point moving average at the pollen collection sites (see Fig. 2).

**Table 1.** The ranges of the a priori distribution of the input parameters used for the inverse simulation in the Surai Khola section.

Parameter	Range
$\Delta T_{\text{jan}}$	[-20, 10] $^{\circ}\text{C}$
$\Delta T_{\text{jul}}$	[-20, 10] $^{\circ}\text{C}$
$\Delta P_{\text{jan}}$	[-90, 100]%
$\Delta P_{\text{jul}}$	[-90, 100]%
Number of iterations	5000

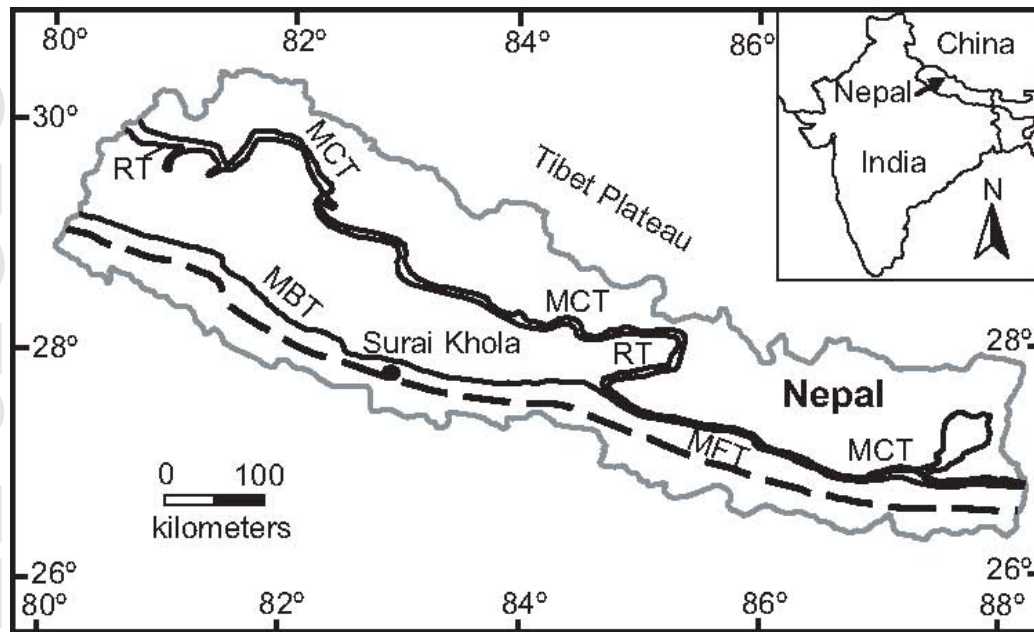
The climate ranges are given in terms of the deviation from the modern values (degrees for temperatures and percentages for precipitation).  $T_{\text{jan}}$ : January temperature;  $T_{\text{jul}}$ : July temperature;  $P_{\text{jan}}$ : January precipitation;  $P_{\text{jul}}$ : July precipitation.

**Table 2.** Regression coefficients between the reconstructed climates for China, using the inverse model, and the observed meteorological values.

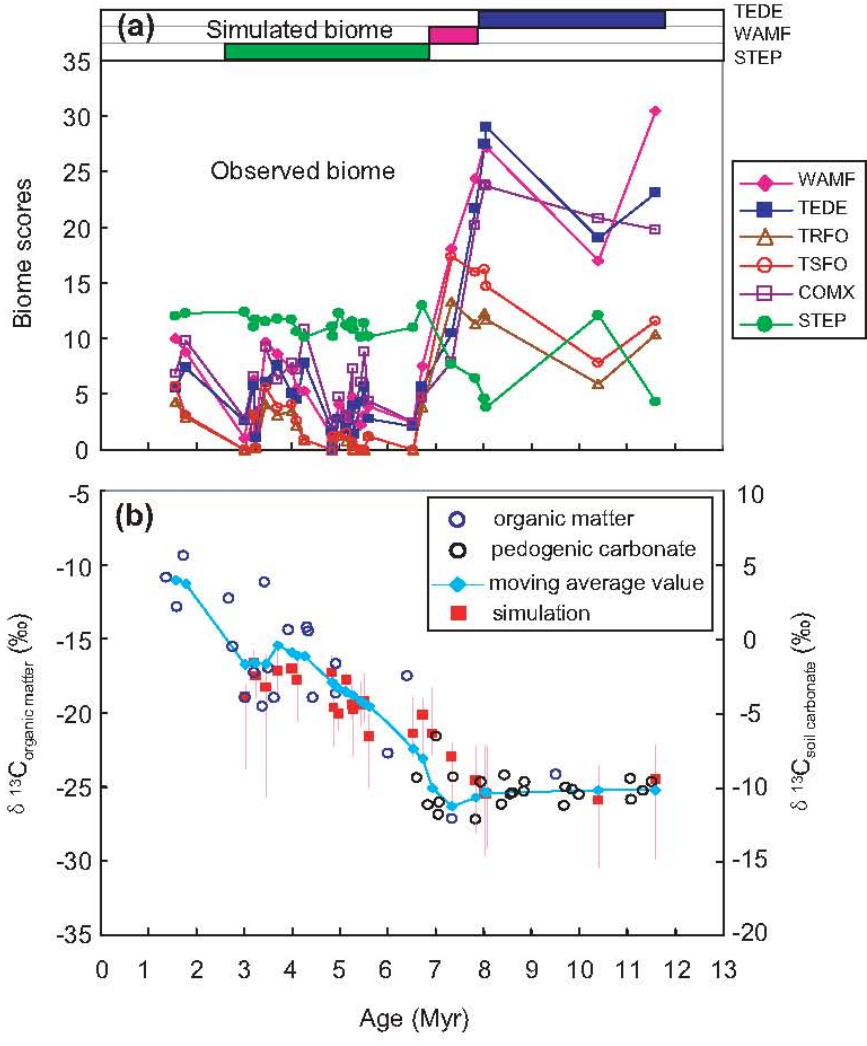
Climate proxy	Slope	Intercept	<i>R</i>	ME	RMSE
Mean annual temperature	$0.82 \pm 0.02$	$0.92 \pm 0.18$	0.89	0.16	3.25
Mean temperature of the coldest month	$0.81 \pm 0.01$	$-1.79 \pm 0.18$	0.95	-0.17	3.19
Mean temperature of the warmest month	$0.75 \pm 0.03$	$4.57 \pm 0.60$	0.75	-0.19	4.02
Total annual precipitation	$1.15 \pm 0.02$	$32.90 \pm 18.41$	0.94	138.01	263.88
Precipitation in January	$1.01 \pm 0.02$	$0.32 \pm 0.47$	0.94	0.52	8.89
Precipitation in July	$1.30 \pm 0.03$	$-21.67 \pm 4.52$	0.89	16.45	52.90
Growing degree-days above $5^{\circ}\text{C}$	$0.74 \pm 0.02$	$464.16 \pm 48.68$	0.89	-106.69	693.60
Ratio of actual to potential evapotranspiration	$0.87 \pm 0.03$	$8.84 \pm 1.42$	0.82	3.06	13.18

*R* is the correlation coefficient ( $\pm$  standard error). ME is the mean value of the residuals. RMSE is the root-mean-square error. These values are calculated based on 482 observations.

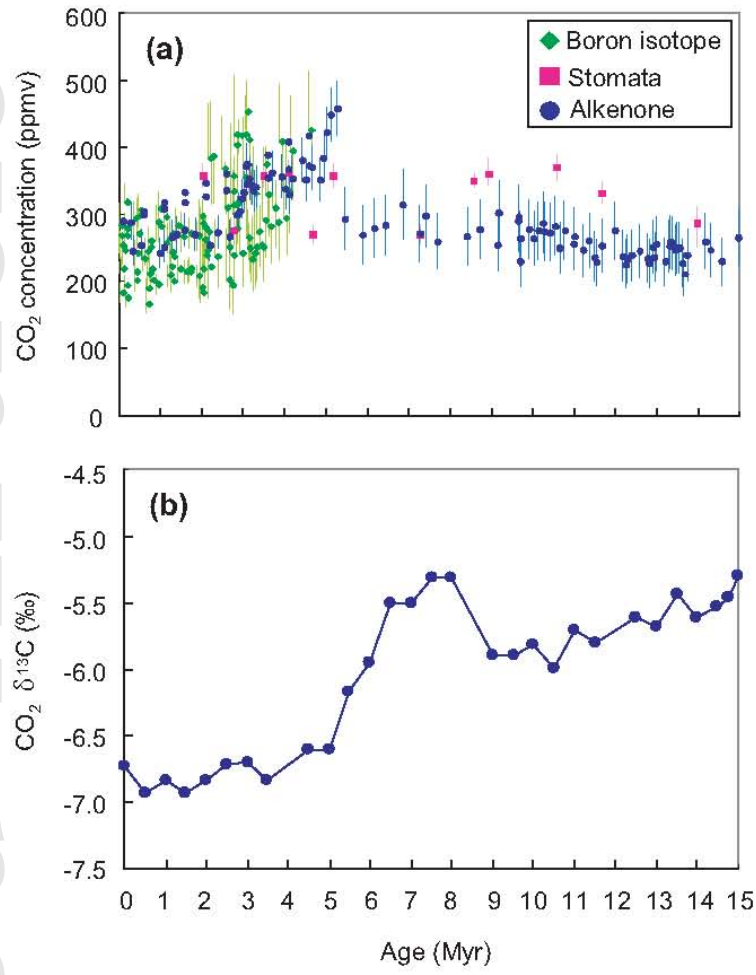
This article is protected by copyright. All rights reserved.



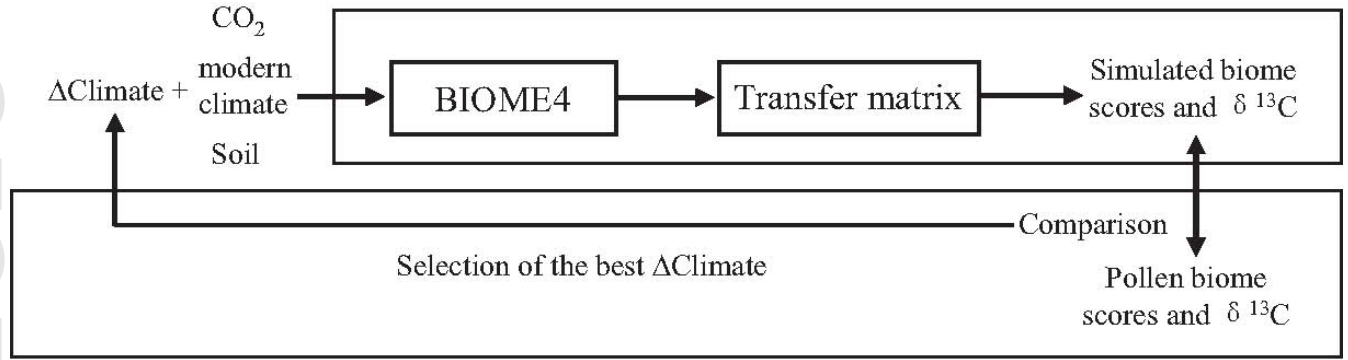
Wu et al\_Fig.1



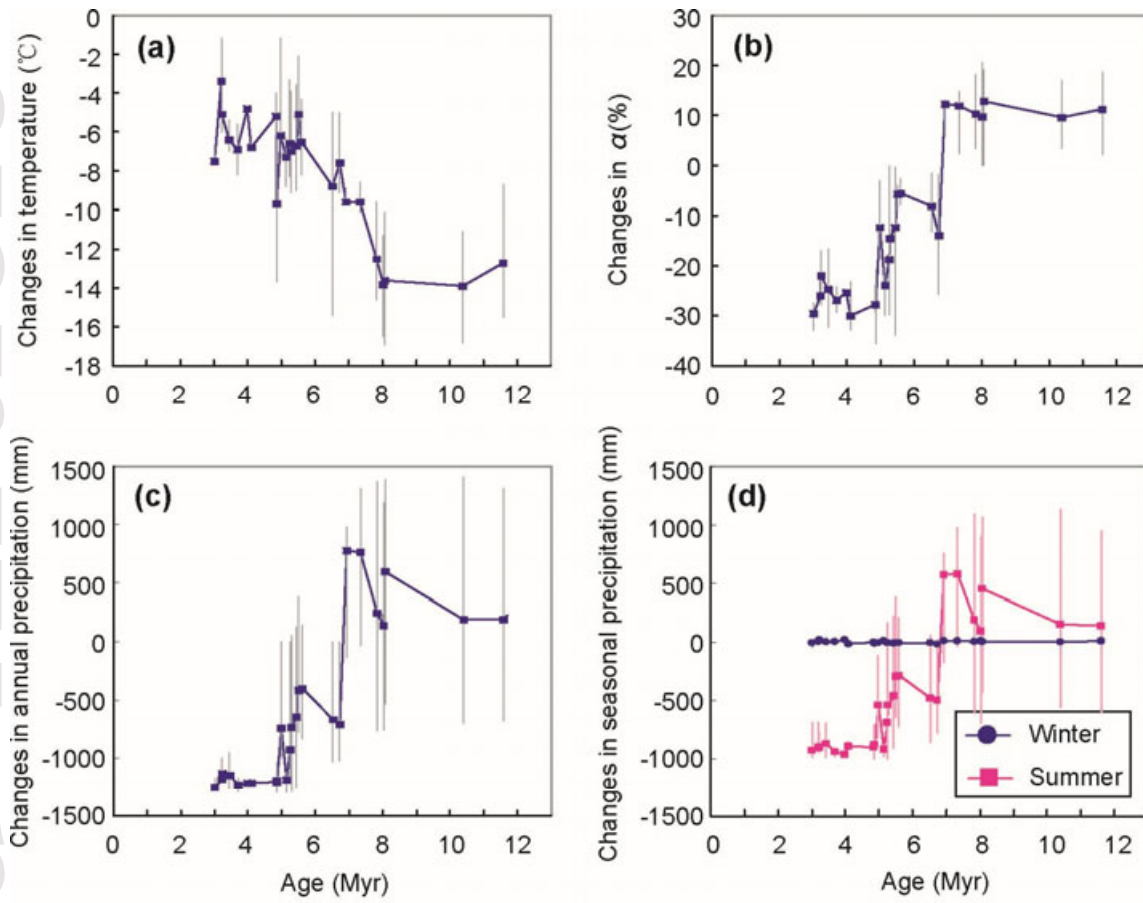
Wu et al\_Fig.2



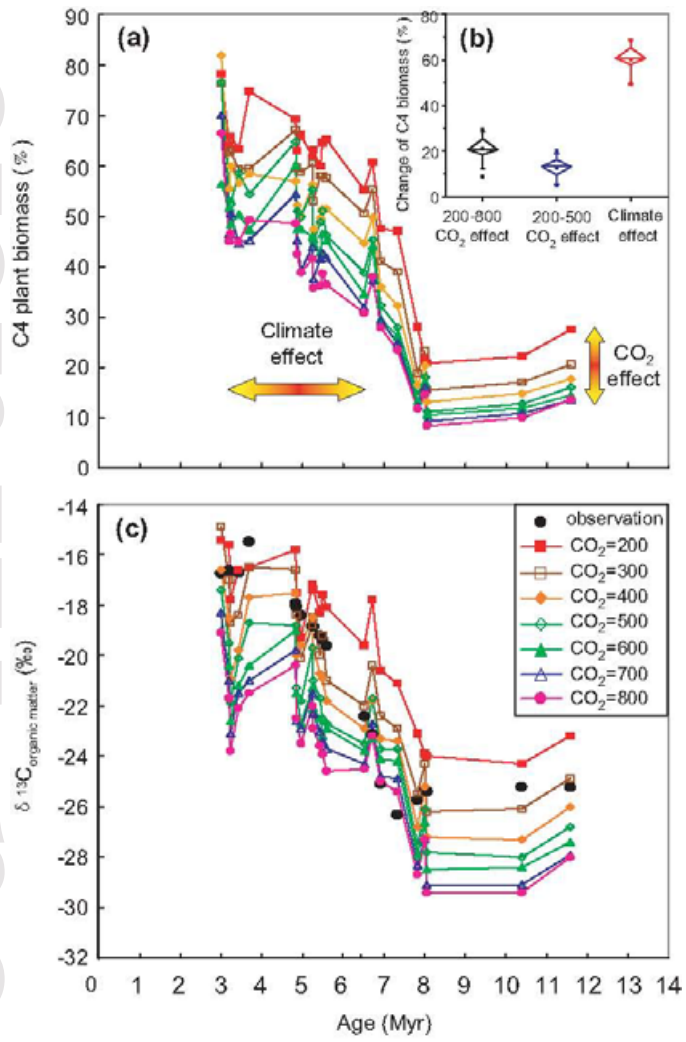
Wu et al\_Fig.3



Wu et al\_Fig . 4



Wu et al\_Fig.5



Wu et al\_Fig.6